

## Comparison of error estimation methods and adaptivity for plane stress/strain problems

Mustafa Özakça†

*Department of Civil Engineering, University of Gaziantep, 27310 Gaziantep, Turkey*

*(Received November 13, 2001, Revised January 7, 2003, Accepted February 21, 2003)*

**Abstract.** This paper deals with adaptive finite element analysis of linearly elastic structures using different error estimators based on flux projection (or best guess stress values) and residual methods. Presentations are given on a typical  $h$ -type adaptive analysis, a mesh refinement scheme and the coupling of adaptive finite element analysis with automatic mesh generation. Details about different error estimators are provided and their performance, reliability and convergence are studied using six node quadratic triangular elements. Several examples are presented to demonstrate the reliability of different error estimators.

**Key words:** finite element; error estimation; adaptivity; plane stress/strain.

---

### 1. General perspective

The finite element (FE) method is now firmly established as a crucial tool for the engineering analyst with applications to endless variety of problems. New methods and capabilities are constantly involving and finding their way into commercial software packages. However, designers who do not have comprehensive expertise in numerical analysis may not even be aware that all FE results are approximate. The FE method is a powerful numerical tool, which is often misused; especially with respect to discretization errors arising from poor mesh design.

We may pose the question now: 'How does an analyst know what constitutes an acceptable mesh in practical analysis?' Recent developments indicate that the discretisation error and its distribution in a FE analysis may be improved using adaptivity. For example, Zienkiewicz and Zhu (1992) have introduced a simple error estimator based on superconvergent FE stresses. Babuska and Rheinboldt (1978) have developed error estimators based on stress jumps around element boundaries and the residual terms in the governing equilibrium equation. Babuska and Yu (1986) and Baehmann *et al.* (1990) introduced the hierarchical shape function concept for error estimation based on previous work by Babuska and Rheinboldt (1978). Babuska and coworkers (1994) discussed computational methodologies for checking the quality of a posteriori error estimators. The methodology accounted precisely for the factors, which affect the quality of error estimators for finite element solutions of linear elliptic problems, namely, the local geometry of the grid and the structure of the solution. Now, it becomes possible to use error estimation to introduce acceptable new meshes leading to

---

† Doctor

solutions with prescribed accuracy.

The use of adaptive mesh refinement (AMR) analysis concept in shape optimisation (Hinton *et al.* 1991), in plate and shell analysis (Cho and Oden 1996, Hinton *et al.* 1991), and in metal forming (Zienkiewicz *et al.* 1988) has been shown to increase the accuracy of the analysis. Research on adaptive analysis of dynamic and non-linear problems is also progressing (Dutta and Ramakrishnan 1997, Stephen and Steven 1997, Mathisen and Okstad 1999).

In the next section, general aspects of adaptive mesh refinement procedure are presented. Governing equations of elasticity and FE approximation are then outlined. Next, the error estimator based on *best guess* solutions and the error energy norm is presented. This paper closes with a few examples where the adaptivity process is tested with respect to its efficiency and convergence characteristics in a global error energy form and in a point wise way to recover displacement or stress values on the boundary.

## 2. General aspects of adaptive mesh refinement procedure

To improve the reliability of the FE method and to ensure that the results produced are of appropriate accuracy, it is essential to estimate the global error as well as the local error distribution in the completed analysis (Zienkiewicz and Zhu 1992). The global error can only serve as a control parameter, the local error distribution indicates the amount of refinement and coarsening necessary to reduce the discretization error.

Optimal meshes are designed by directly predicting the mesh sizes based on a local error estimate. The predicted optimal mesh can be generated by using an automatic mesh generator, by successive mesh enrichment or by mesh movement (Sienz 1994).

In this work, the optimal mesh is generated using an automatic mesh generator. The automatic AMR procedure performs the initial analysis and subsequent re-analyses without any user intervention until the error in the solution reaches a desired accuracy. The basic AMR procedure is as follows.

1. Produce a starting mesh and carry out an initial FE analysis.
2. Based on the results of the FE analysis, evaluate the error estimate.
3. If the error estimate is acceptable then the adaptive analysis is complete; otherwise continue
4. Re-mesh the whole domain based on a new mesh density evaluated using error distribution.
5. Perform the FE analysis again based on the new mesh and go to step 2.

As can be seen, an adaptive scheme is composed of two main ingredients (Strouboulis and Haque 1992): Thus an AMR scheme is composed of three main ingredients:

- *Error estimation*: this includes the methods and algorithms used for the estimation of the error in approximate solutions. The results of an a posteriori error analysis may be employed to check if the quality of an approximate solution meets tolerances specified by an analyst and may also be used to derive the adaptive scheme which optimises the structure of the approximation.
- *Mesh re-design*: This refers to the methods, which are used to predict the optimal distribution of the parameters of the approximation based on the error-estimated error and the procedures which are employed in the adaptation of the approximation. The mesh is modified using an adaptive scheme, which is a set of procedures employed to control the parameters of the approximation.

This combination forms a practical, reliable and versatile algorithm, which can be used for both research and industrial purposes and can be attached to the FE analysis code with minor modifications.

### 3. Governing equations of elasticity

In order to describe the error estimators adopted in the current work we briefly review the sources of discretization error. The governing equilibrium equations of elasticity may be expressed as

$$\mathbf{L}\boldsymbol{\sigma} - \mathbf{b} = \mathbf{0} \tag{1}$$

in a domain  $\Omega$ , subject to the conditions

$$\mathbf{u} = \bar{\mathbf{u}} \text{ on the boundary } \Gamma_u, \text{ and}$$

$$\mathbf{t} = \bar{\mathbf{t}} \text{ on the boundary } \Gamma_t$$

where  $\boldsymbol{\sigma}$  is the ‘vector’ of stresses,  $\mathbf{u}$  is the vector of displacement fields,  $\mathbf{L}$  is a matrix of differential operators,  $\mathbf{b}$  is the vector of body forces,  $\bar{\mathbf{u}}$  is the vector of prescribed displacements on boundary  $\Gamma_u$  and  $\bar{\mathbf{t}}$  is the vector of prescribed tractions on boundary  $\Gamma_t$ . The strains  $\boldsymbol{\varepsilon}$  may then be calculated from the expression

$$\boldsymbol{\varepsilon} = \mathbf{L}^T \mathbf{u} \tag{2}$$

and the stresses  $\boldsymbol{\sigma}$  can be evaluated as

$$\boldsymbol{\sigma} = \mathbf{D}\boldsymbol{\varepsilon} \tag{3}$$

where  $\mathbf{D}$  is the elastic modulus matrix.

### 4. Finite element approximation

Detailed treatment of the standard FE formulation can be found in many text books (Zienkiewicz and Taylor 2000, Cook *et al.* 1989). In this section, however, only the fundamental principles required by subsequent parts of the present work are outlined.

The basic concept of the FE method is that a continuum can be modelled numerically by subdividing it into discrete regions or *finite elements* interconnected at *nodal points*. It is assumed that the general behaviour of the continuum can be expressed in terms of a finite number of parameters or nodal values. To this end, *isoparametric* elements use a single set of functions to interpolate both the geometry and field variables inside each element from a respective set of nodal values. These interpolation functions, the *shape functions*, are defined for a parent element in a *natural* coordinate system  $(\xi, \eta)$  the axes of which have values ranging from  $-1$  to  $1$ .

In the FE *displacement approach*, which is adopted exclusively in this work, nodal displacements are the primary unknown to be computed (stress is a secondary variable computed from the displacements). Let the displacements  $\mathbf{u}$  at any point within the element  $e$  be approximated as a column vector  $\hat{\mathbf{u}}$  :

$$\mathbf{u} \approx \hat{\mathbf{u}} = \mathbf{N}\mathbf{d}^e = \sum_{i=1}^n \mathbf{N}_i \mathbf{d}_i \quad (4)$$

where  $\hat{\mathbf{u}}$  is the FE approximation to  $\mathbf{u}$ ,  $\mathbf{d}^e$  is the vector of nodal displacements for a particular element,  $n$  is the number of nodes per element,  $\mathbf{N}$  is the matrix of shape functions and is a diagonal matrix of  $n$  submatrices  $\mathbf{N}_i = \mathbf{N}_i \mathbf{I}$  with  $\mathbf{I}$  being a  $2 \times 2$  identity matrix.  $N_i$  is the shape function associated with node  $i$ . In the case of plane stress,

$$\mathbf{u} = \begin{bmatrix} u(x, y) \\ v(x, y) \end{bmatrix} \quad (5)$$

represents the horizontal and vertical displacements of a typical point within the element and

$$\mathbf{d}_i = \begin{bmatrix} u_i \\ v_i \end{bmatrix} \quad (6)$$

the corresponding displacement of a node  $i$ . To calculate the displacements  $u(\xi, \eta)$  and  $v(\xi, \eta)$  at any point within the element, we make use of the expressions

$$u(\xi, \eta) = \sum_{i=1}^n N_i(\xi, \eta) u_i \quad (7a)$$

$$v(\xi, \eta) = \sum_{i=1}^n N_i(\xi, \eta) v_i \quad (7b)$$

The strain vector may then be calculated from the expression

$$\hat{\boldsymbol{\varepsilon}} = \mathbf{L}^T \mathbf{N} \mathbf{d}^e \equiv \mathbf{B} \mathbf{d}^e = \sum_{i=1}^n \mathbf{B}_i \mathbf{d}_i \quad (8)$$

where  $\mathbf{B}$  is termed the strain-displacement matrix. In its simplest linear form, the  $\mathbf{B}$  matrix consists of the Cartesian derivatives of the shape functions.

The isoparametric concept allows the geometry of the element to be expressed in terms of its nodal coordinates by means of the same set of shape functions  $N_i$  used in the interpolation of displacements. For instance at any point  $(\xi, \eta)$  within an isoparametric element. The  $x$  and  $y$  coordinates may be obtained from the expressions

$$x(\xi, \eta) = \sum_{i=1}^n N_i(\xi, \eta) x_i \quad (9a)$$

$$y(\xi, \eta) = \sum_{i=1}^n N_i(\xi, \eta) y_i \quad (9b)$$

The shape functions  $N_i$  are given in terms of natural coordinates  $(\xi, \eta)$ , but the  $\mathbf{B}$  matrix requires derivatives of  $N_i$  with respect to the global coordinates  $x$  and  $y$ . The transformation between the two

coordinate systems is accomplished by means of the Jacobian matrix,  $\mathbf{J}$ , which is given by

$$\mathbf{J} = \begin{bmatrix} \partial x / \partial \xi & \partial y / \partial \xi \\ \partial x / \partial \eta & \partial y / \partial \eta \end{bmatrix}. \quad (10)$$

Finally, the stresses may be related to the strains by use of an elasticity matrix  $\mathbf{D}$  as follows

$$\hat{\boldsymbol{\sigma}} = \mathbf{D}\mathbf{B}\mathbf{d}^e \quad (11)$$

To check for satisfaction of the governing equilibrium equations we substitute  $\hat{\boldsymbol{\sigma}}$  given by Eq. (11) into Eq. (1) and obtain

$$\mathbf{L}^T \hat{\boldsymbol{\sigma}} - \mathbf{b} = \mathbf{r} \neq \mathbf{0} \quad (12)$$

where  $\mathbf{r}$  is a vector of residual body forces. Evaluation of the residual forces for a plane stress problem and explicit equations of the residual forces for plane strain and axisymmetric problems are given in Appendix A.

## 5. Error estimation

We now focus our attention on the local and global error estimation. The *global* error estimate allows us to determine, for the mesh currently being used, whether we have satisfied our main objective of reducing the global error to a certain specified value. On the other hand, if the global error is not low enough, then the *local* contribution of the error to the global error estimate provides us with information on how the current mesh can be refined to efficiently reduce the global error. There are two main groups of methods:

- residual-based methods and
- flux projection (or best guess stress) methods.

In order to normalise these error measures they are usually divided by the strain energy  $\|\mathbf{w}\|$ . We now describe a selection of algorithms from both sets of methods

### 5.1 Residual based methods

In this section we consider two residual-based methods:

- the element residual method and
- the sub-domain method.

#### 5.1.1 Element residual method

The FE solution gives an approximate displacement field, which is continuous over the domain. However, the derivatives of this field are discontinuous across element boundaries. These discontinuities in the displacement derivatives imply strain and hence stress jumps across element boundaries (Babuska and Rheinboldt 1978, Kelly *et al.* 1983). Various error estimators use the inter-element traction jump around the element boundary and the residual terms in the governing equation over the interior of the element to obtain an error estimate. Techniques using energy norms

derived by several authors (Babuska and Rheinboldt 1978, Kelly *et al.* 1983) have the general form

$$\|e\| = (C_1 \int_{\Omega} \mathbf{r}^T \mathbf{r} d\Omega + C_2 \int_I \mathbf{j}^T \mathbf{j} dI)^{1/2} \quad (13)$$

where  $\Omega$  is the total domain,  $C_1$  and  $C_2$  are constants,  $I$  is the total interface between elements,  $\mathbf{j}$  are the inter-element tractions and  $\mathbf{r}$  are the residual forces and can be obtained from Eq. (12). A particular expression derived in Kelly *et al.* (1983) for two-dimensional problems defines an element contribution to  $\|e\|$  as

$$\|e\|_i = \left( \frac{h^2}{24K} \int_{\Omega_e} \mathbf{r}^T \mathbf{r} d\Omega + \frac{h}{24K} \int_I \mathbf{j}^T \mathbf{j} dI \right)^{1/2} \quad (14)$$

where  $h$  is the element size and  $K$  is dependent on the problem being solved: for plane stress

$$K = \frac{E}{(1 - \nu)} \quad (15)$$

and for plane strain and axisymmetric problems

$$K = \frac{E}{(1 + \nu)(1 - 2\nu)} \quad (16)$$

where  $E$  is Young's modulus and  $\nu$  is Poisson's ratio.

The interior residual term in Eq. (13) is the dominant error term when the shape functions consist of piecewise biquadratic functions. However, the dominant error term in Eq. (13) is the boundary term when the shape functions consist of piecewise bilinear functions. Thus the boundary term can be neglected when estimating errors of biquadratic FE approximations (Babuska and Rheinboldt 1978). Furthermore, Babuska and Yu (1986) have recently shown more generally that for odd-degree elements (elements with odd-degree polynomial shape functions), the inter-element traction jumps dominate the error, but for even degree elements, the interior residuals will be dominant. Recently, Robinson and Armstrong (1992) made use of the interior residual term and the boundary term using 8-noded isoparametric elements. They have carried out the analysis for different linearly and quadratically loaded plane stress/strain problems where the exact analytical solution is known. They have also found that the interior residual term is the dominant term and the boundary term is negligible.

The error estimation scheme in this section uses these results to estimate the error energy  $\|e\|$  of piecewise quadratic approximations in meshes of 6-noded triangular elements. The approach taken is to calculate only the interior residual portion of the error in the elements by neglecting the boundary term in Eq. (13).

$$\|e\|_i = (C_1 \int_{\Omega_e} \mathbf{r}^T \mathbf{r} d\Omega)^{1/2} \quad (17)$$

### 5.1.2 Sub-domain method

Another residual error estimator which makes use of residual  $\mathbf{r}$  using a solution based on hierarchical bubble functions has been described by Babuska and Yu (1986). Baehmann *et al.* (1990) have applied to two and three dimensional elasticity problems. This method is now presented.

In this scheme we first evaluate the interior residual body forces  $\mathbf{r}$  obtained when the FE stresses are substituted into the governing differential Eq. (12). For the 6-noded triangular element we assume that there exists a better solution based on quartic variations of the displacements over the element. Thus we represent the error  $\mathbf{e}$  in the displacements using hierarchical (quartic) bubble functions so that

$$\mathbf{e} = \sum_{i=1}^3 \tilde{N}_i \mathbf{g}_i \tag{18}$$

where  $\tilde{N}_i = \tilde{N}_i \mathbf{I}_2$  and the shape functions  $\tilde{N}_i$  are written as

$$\begin{aligned} \tilde{N}_1 &= \xi\eta(1 - \xi - \eta) \\ \tilde{N}_2 &= \xi^2\eta(1 - \xi - \eta) \\ \tilde{N}_3 &= \xi\eta^2(1 - \xi - \eta) \end{aligned} \tag{19}$$

$\mathbf{g}_i$  are unknown nodeless coefficients associated with the distribution of the displacement error  $\mathbf{e}$  within the element.

To obtain these coefficients we solve the stiffness equations for the element, which have the form

$$\tilde{\mathbf{K}}\mathbf{g} = \mathbf{f}_r \tag{20}$$

where the stiffness matrix  $\tilde{\mathbf{K}}$  has the form

$$\tilde{\mathbf{K}} = \int_{\Omega_i} [L\tilde{\mathbf{N}}]^T \mathbf{D} [L\tilde{\mathbf{N}}] d\Omega \tag{21}$$

and  $\tilde{\mathbf{N}} = [\tilde{N}_1 \ \tilde{N}_2 \ \tilde{N}_3]$ . The consistent nodal forces  $\mathbf{f}_r$  associated with the residual error body forces  $\mathbf{r}$  may be expressed as

$$\mathbf{f}_r = \int_{\Omega_i} [\tilde{\mathbf{N}}]^T \mathbf{r} d\Omega \tag{22}$$

and the vector of the unknown coefficients  $\mathbf{g} = [\mathbf{g}_1^T \ \mathbf{g}_2^T \ \mathbf{g}_3^T]^T$ . We now make the following remarks concerning the sub-domain method:

1. Since the shape functions are quartic, a 13-point integration rule is needed to  $\tilde{\mathbf{K}}$ .
2. For the quadratic 6-noded element the residual body forces are uniformly distributed over each element.
3. The strain energy error for element  $i$  associated with the quartic displacements is obtained for the expression

$$\|\mathbf{e}\|_{\Omega_i}^2 = \frac{1}{2} \mathbf{g}^T \tilde{\mathbf{K}} \mathbf{g} \tag{23}$$

4. The total error energy which is used to evaluate the global percentage error is obtained from

$$\|\mathbf{e}\|_{\Omega}^2 = \sum_{i=1}^n \|\mathbf{e}\|_{\Omega_i}^2 \tag{24}$$

## 5.2 Flux projection (or best guess stress) methods

In this section we consider a set of algorithms known as flux projection methods (Zienkiewicz and Zhu 1992). These methods make use of an error energy norm of the form

$$\|e\| = \left( \int_{\Omega} [\boldsymbol{\sigma} - \hat{\boldsymbol{\sigma}}]^T \mathbf{D}^{-1} [\boldsymbol{\sigma} - \hat{\boldsymbol{\sigma}}] d\Omega \right)^{1/2} \quad (25)$$

where  $\boldsymbol{\sigma}$  are the exact stresses and  $\hat{\boldsymbol{\sigma}}$  are the ‘row’ FE stresses. As we do not have access to the exact stresses  $\boldsymbol{\sigma}$ , we substitute our best guess stresses  $\boldsymbol{\sigma}^*$ . By *best guess*, we mean that the stresses  $\boldsymbol{\sigma}^*$  are as close as possible to the exact stresses  $\boldsymbol{\sigma}$ , so that

$$\boldsymbol{\sigma} \approx \boldsymbol{\sigma}^* \quad (26)$$

The ‘row’ FE stresses  $\hat{\boldsymbol{\sigma}}$  are usually discontinuous across element interfaces. There are various methods for producing more accurate and continuous stress fields  $\boldsymbol{\sigma}^*$ . The object of this section is to describe these methods, which can then be used in conjunction with Eq. (25) to produce contributions to  $\|e\|$  from each element. Before choosing one of these stress recovery techniques, it is necessary to give answers to a number of important questions which arise in connection with the use of different elements:

- Stresses may be evaluated at any point within the element domain. Which points are the most convenient to the engineer who must use the results of the computer analysis to interpret the behaviour and integrity of the structure?
- At which points within the element are the stresses most accurately determined? And as a corollary of this, which points are the least accurate?
- Can the oscillatory nature of the stresses be damped out to obtain a smoothly varying continuous stress field?
- Are smoothed stresses always desirable?

It is usually accepted that the nodal values are the most convenient location for sampling of stresses and these also facilitate error estimation and sensitivity analysis procedures. However, it is also fairly well known that interpolation functions are usually less accurate towards the extremities of the interpolation region. (For the finite element case the nodes are at the extremities of the region.) Bearing this in mind, the stresses may be smoothed to reduce or eliminate oscillations.

Several simple methods have been proposed in the past and are widely used in practice. These are:

- nodal averaging,
- least squares smoothing,
- superconvergent patch recovery method and,
- Loubignac iteration.

All of which have been considered in the present study and will now be described.

### 5.2.1 Nodal averaging

The simplest known form of smoothing is averaging of the nodal stresses<sup>1</sup>  $\hat{\boldsymbol{\sigma}}_i^{(e)}$  at each node.

<sup>1</sup>We deal with each stress component (e.g.,  $\sigma_x$ ,  $\sigma_y$ ,  $\tau_{xy}$ ) in turn.

Smoothed stresses for each node are obtained by averaging the stress contributions of all elements connected to that node.

$$\sigma_i^* = \frac{\sum_e \hat{\sigma}_i^{(e)}}{n} \tag{27}$$

in which  $\hat{\sigma}_i^{(e)}$  is the stresses at node  $i$  of element  $e$  and  $n$  is the number of elements meeting at node  $i$ .

This averaging process may be applied to the unsmoothed nodal stresses or to the locally smoothed nodal stresses. For simple elements with linear variation of displacements, the simple nodal averaging is adequate, for more complex elements, such as quadratic or cubic isoparametric elements; other methods which lead to improved best guesses approximation are worthy of consideration.

### 5.2.2 Least squares smoothing

Least square smoothing is now considered. The component of the continuous stress field  $\sigma^*$ , which is approximated as

$$\sigma^* = \sum_i N_{\sigma_i} \sigma_i^* \tag{28}$$

where  $N_{\sigma_i}$  is a  $C^0$  continuous shape function and  $\sigma_i^*$  is the smoothed nodal stress associated with node  $i$ . The continuous stress  $\sigma^*$  is determined by forcing the Galerkin-like condition

$$\int_{\Omega} N_{\sigma_i} (\sigma^* - \hat{\sigma}) d\Omega = 0 \tag{29}$$

As numerical integration techniques are typically employed, therefore, the finite element stress values  $\hat{\sigma}$  used in the smoothing process are evaluated at the integration points which, in the case of Gauss-Legendre quadrature are typically the most accurate locations in the element for their evaluation. Eq. (29) is equivalent to the least squares smoothing procedure of Hinton and Campbell (1974).

One method, which can be employed to obtain a continuous stress field using Eqs. (28) and (29) is to assume that the stress  $\sigma^*$  is interpolated by the same shape function  $N_i$  as the individual displacement components. Note that other shape functions (e.g., functions, which are one order less than  $N_i$  may also be used. This yields

$$S \sigma^* - q = \mathbf{0} \tag{30}$$

where typical components may be written as

$$S_{ij} = \int_{\Omega} N_i N_j d\Omega \quad \text{and} \quad q_i = \int_{\Omega} N_i \hat{\sigma} d\Omega \tag{31}$$

and

$$\sigma^* = [\sigma_1^*, \sigma_2^*, \dots]^T \tag{32}$$

are the smoothed nodal values of the nodes. For local least squares smoothing, Eq. (30) is solved by considering individual element domains separately.

To reduce the solution cost in global least squares smoothing, the stress smoothing matrix  $S$  can be diagonalised. This reduces the effort required to solve Eq. (30) to one division operation for each stress component at each node. Implementation of this method is very easy --- for example the terms of a row may be simply summed to the diagonal. However, if the  $S$  matrix for the 6 noded triangular elements is lumped in this manner, the terms representing the corner nodes will be negative. Thus, the smoothing matrix loses its positive definite character. Hinton *et al.* (1976) have proposed a lumping scheme, which yields a positive definite smoothing matrix. The total area of the element is divided among the nodes in proportion to the diagonal terms of the consistent  $S$  matrix and the shape functions are assumed to have unit value within this region and zero elsewhere.

### 5.2.3 Superconvergent patch recovery technique

As mentioned above, the stresses  $\hat{\sigma}$  calculated from Eq. (11) do not possess interelement continuity and have a low accuracy at the nodal points and boundaries of finite elements.

The nodal value of a typical stress component in the superconvergent patch recovery process can be sampled from a polynomial expansion  $\hat{\sigma}^*$  of the same order as that present in the element interpolation functions (Zienkiewicz and Zhu 1992) and which extends over an element patch, i.e., a set of element meeting at a common corner nodal point as shown in Fig. 1. The polynomial function  $\hat{\sigma}^*$  is written as

$$\hat{\sigma}^* = Pa \quad (33)$$

where  $P$  contains the polynomial terms and  $a$  are the unknowns. The order of the smoothing function or the polynomial terms  $P$  is usually of the same order as the element shape functions so that for the 6-noded triangular elements adopted here, for example, quadratic smoothing functions are used and

$$P = [1, x, y, x^2, xy, y^2] \quad (34)$$

The unknowns  $a$  are obtained using a local least squares fit to the stresses sampled at the integrating (or superconvergent points) of an element patch. This is done by minimising the sum of the squares of errors in the stress

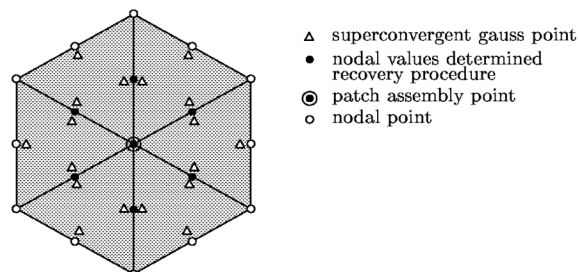


Fig. 1 Computation of superconvergent nodal values for 6-noded quadratic triangular elements

$$\begin{aligned}
 F(\mathbf{a}) &= \sum_{i=1}^n [\hat{\sigma}(x_i, y_i) - \sigma^*(x_i, y_i)]^2 \\
 &= \sum_{i=1}^n [\hat{\sigma}(x_i, y_i) - \mathbf{P}(x_i, y_i)\mathbf{a}]^2
 \end{aligned}
 \tag{35}$$

where  $(x_i, y_i)$  are the coordinates of the sampling points and  $n$  is the total number of sampling points in a patch. The minimisation of Eq. (35) leads an explicit expression for  $\mathbf{a}$  of the form

$$\mathbf{a} = \mathbf{A}^{-1}\mathbf{b}
 \tag{36}$$

where

$$\begin{aligned}
 \mathbf{A} &= \sum_{i=1}^n \mathbf{P}^T(x_i, y_i)\mathbf{P}(x_i, y_i) \\
 \mathbf{b} &= \sum_{i=1}^n \mathbf{P}^T(x_i, y_i)\hat{\sigma}(x_i, y_i)
 \end{aligned}
 \tag{37}$$

Once the unknowns  $\mathbf{a}$  have been calculated, nodal values are obtained by the insertion of the associated nodal coordinates into the expression for  $\sigma^*$ . This recovery technique is performed for each nodal vertex.

It can be expected that all values of  $\sigma^*$  in the domain of the patch are superconvergent. The convergence and reliability of the superconvergent patch recovery technique is illustrated later for several adaptivity examples. Also some results obtained using conventional smoothing and the superconvergent patch recovery technique are compared.

The stress sampling points is shown in Fig. 1 for quadratic triangular elements. However, for triangular elements the existence and the locations of superconvergent points are still matters which do not appear to have been fully explored mathematically despite the early work of Moan (1974) suggesting the existence of optimal integration points. It is suggested that some of the derivatives are superconvergent at midside nodes of triangular element (Zienkiewicz and Zhu 1992, Moan 1974,

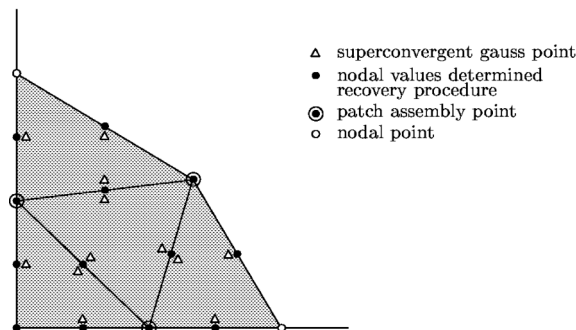


Fig. 2 Computation of superconvergent nodal values for boundary nodes

Barlow 1976). In the present work, stresses are sampled at the three midside nodes.

It will be observed that element patches will overlap for midside nodes. This means that such recovered nodal values are evaluated from two patches except at the boundaries of the mesh. As all such values are superconvergent, nodal averaging is used at these points. The recovered vertex nodal values are, however, only determined from a single patch.

A more difficult situation arise at the boundary of the domain where a local patch, such as the one illustrated in Fig. 2, may involve only one or two elements. For the one element situation (corner point) the size of patch is insufficient for determination of the parameter  $\mathbf{a}$  and the corner node values are determined from an interior patch. For two element patches the situation is simpler and such patches are assembled and solved in the standard manner.

#### 5.2.4 Loubignac algorithm

Although the use of continuous stress fields eliminates the traction jumps between elements, it does not guarantee a better satisfaction of the overall equilibrium. In fact, the continuous stress fields obtained using least squares smoothing or simple nodal averaging do not satisfy the overall equilibrium conditions.

The governing equations of static equilibrium for a domain  $\Omega$  with a system of body forces and applied surface tractions can be simply established using *the Principle of Virtual Work* in which

$$\int_{\Omega} \delta \boldsymbol{\varepsilon}^T \boldsymbol{\sigma} d\Omega - \int_{\Omega} \delta \mathbf{u}^T \mathbf{b} d\Omega - \int_{\Gamma_t} \delta \mathbf{u}^T \mathbf{t} d\Gamma = \mathbf{0} \quad (38)$$

where virtual displacements  $\delta \mathbf{u}$  and associated virtual strains  $\delta \boldsymbol{\varepsilon}$  may be represented by the expressions

$$\delta \mathbf{u} = \sum \mathbf{N} \delta \mathbf{d} \quad \text{and} \quad \delta \boldsymbol{\varepsilon} = \sum \mathbf{B} \delta \mathbf{d} \quad (39)$$

The governing FE equations are obtained by substituting Eq. (39) into Eq. (38)

$$\delta \mathbf{d} \left( \int_{\Omega} \mathbf{B}^T \boldsymbol{\sigma} d\Omega - \int_{\Omega} \mathbf{N}^T \mathbf{b} d\Omega - \int_{\Gamma_t} \mathbf{N}^T \mathbf{t} d\Gamma \right) = \mathbf{0} \quad (40)$$

and as Eq. (40) is true for any  $\delta \mathbf{d}$ , we obtain

$$\int_{\Omega} \mathbf{B}^T \boldsymbol{\sigma} d\Omega - \mathbf{f} = \mathbf{0} \quad (41)$$

However, when the continuous stress field  $\boldsymbol{\sigma}^*$  is substituted into Eq. (41), residual nodal forces  $\mathbf{q}$  are obtained

$$\int_{\Omega} \mathbf{B}^T \boldsymbol{\sigma}^* d\Omega - \mathbf{f} = \mathbf{q} \quad (42)$$

These residual forces can be minimised by the application of Loubignac's iteration scheme (Cantin *et al.* 1978). Now, an algorithm is described to obtain a continuous stress field as well as the usual continuous displacement field. It provides an equilibrated stress field in the weak sense (i.e. in the finite element sense). The steps to be followed to implement the proposed algorithm are:

1. Solve the problem by the classical method to obtain the displacements  $\mathbf{d}_0$  and stresses  $\hat{\boldsymbol{\sigma}}_0$  from Eqs. (4) and (11) respectively and set counter  $i = 0$ .
2. Increase the count number by 1 ( $i = i + 1$ ) and calculate smoothed nodal stresses  $\bar{\boldsymbol{\sigma}}_i$  starting from  $\bar{\boldsymbol{\sigma}}_{i-1}$  by global or local smoothing or by nodal averaging, e.g. compute the mean nodal values of stresses  $\hat{\boldsymbol{\sigma}}$ .

$$\bar{\boldsymbol{\sigma}}_i = \frac{1}{n_{se}} \sum_{e=1}^{n_{se}} \hat{\boldsymbol{\sigma}}_{i-1}^{(e)} \quad (43)$$

3. Interpolate the stresses using the nodal values to give a continuous field  $\boldsymbol{\sigma}^*$

$$\boldsymbol{\sigma}_i^* = \mathbf{N} \bar{\boldsymbol{\sigma}}_i \quad (44)$$

4. Evaluate the residual  $\mathbf{q}_i$  from Eq. (42) corresponding to the current stress field  $\boldsymbol{\sigma}_i^*$  defined in 3.
5. Solve

$$\Delta \mathbf{d}_i = -\mathbf{K}^{-1} \mathbf{q}_i \quad (45)$$

6. Update  $\mathbf{d}$  and  $\hat{\boldsymbol{\sigma}}$

$$\mathbf{d}_i = \mathbf{d}_{i-1} + \Delta \mathbf{d}_i \quad (46)$$

$$\hat{\boldsymbol{\sigma}}_i = \mathbf{D} \mathbf{B} \mathbf{d}_i \quad (47)$$

7. Evaluate  $\|\mathbf{q}_i\|$  and check convergence

$$\frac{\|\mathbf{q}_i\|}{\|\mathbf{f}\|} < \delta \quad (48)$$

and go to step 2 if convergence is not obtained.

The convergence is generally fast and 2-6 iterations are normally used.

### 5.3 Estimation of global error

The error energy norms presented in the previous sections are a measure of the absolute value of the predicted error over the domain. The predicted value of the percentage global error  $\eta$  is given by the expression

$$\eta = \frac{\|\mathbf{e}\|}{\|\mathbf{w}\|} \quad (49)$$

is the where  $\|\mathbf{w}\|$  strain energy of the exact solution. In Zienkiewicz and Zhu (1992) the exact strain energy norm of the solution is approximated by

$$\|\mathbf{w}\| \cong \|\mathbf{w}^*\| \quad (50)$$

where

$$\|\mathbf{w}^*\| \equiv (\|\hat{\mathbf{w}}\|^2 + \|\mathbf{e}\|^2)^{1/2} \quad (51)$$

in which  $\|\hat{\mathbf{w}}\|$  is the FE approximation to the strain energy norm and is defined as

$$\|\hat{\mathbf{w}}\| = \left( \int_{\Omega} \hat{\boldsymbol{\sigma}}^T \mathbf{D}^{-1} \hat{\boldsymbol{\sigma}} d\Omega \right)^{1/2} \quad (52)$$

Alternatively, Özakça (1993) approximate  $\|\mathbf{w}^*\|$  using the ‘smoothed’ continuous stress field

$$\|\mathbf{w}^*\| = \left( \int_{\Omega} [\boldsymbol{\sigma}^*]^T \mathbf{D}^{-1} \boldsymbol{\sigma}^* d\Omega \right)^{1/2} \quad (53)$$

since the strain energy of the FE solution  $\|\hat{\mathbf{w}}\|^2$  can be upper or lower bounded by the exact strain energy. The estimation given by Eq. (51) is not valid if  $\|\hat{\mathbf{w}}\|^2$  is lower bounded.

Eq. (49) allows an effective adaptive process to be developed with the principle objective of achieving a specified overall percentage accuracy  $\bar{\eta}$  --- say 5% in many engineering applications (Zienkiewicz and Taylor 2000). Thus, if for a given mesh we find that

$$\eta > \bar{\eta} \quad (54)$$

then we must refine the mesh in order to reduce  $\eta$ . In the next section we consider a strategy developed by Zienkiewicz and Zhu (1992) to achieve this.

## 6. Refinement procedure

### 6.1 Refinement indicators

The essential question to be considered in this section is the identification of the adaptive principles on which the decision for the refinement will be based. The main principle in  $h$ -refinement is to refine the mesh so as to equally distribute the global error within each element and to reduce the total error to an acceptable user-specified level.

As the aim is to obtain a uniform error distribution for all elements, the permissible error for each element is determined by

$$\bar{\rho} = \frac{\bar{\eta} \|\mathbf{w}^*\|}{n_{el}^{1/2}} \quad (55)$$

where  $n_{el}$  is the total number of elements in the domain under investigation. As the error is evaluated at the element level, we define the parameter  $\xi_i$  for each element as

$$\xi = \frac{\|e\|_i}{\bar{\rho}} \quad (56)$$

where  $\xi_i$  is called ‘refinement indicator’. Depending on the values of  $\xi_i$  we can identify three possible element states:

- if  $\xi_i = 1$  optimal element size
- if  $\xi_i > 1$  refinement is necessary, and
- if  $\xi_i < 1$  de-refinement is possible.

More recently, Onate *et al.* (1992) proposed a new method for mesh density evaluation<sup>2</sup>. However, this method leads to many elements at the final solution and solution may not converge if singularity points exist. In the present work the first approach is used which is mesh optimality based on equal distribution of global error within each element.

### 6.2 Evaluation of the mesh density

The characteristic feature of the AMR procedure is the use of the current solution to predict the new mesh size  $\bar{h}_i$ . For instance, if the current element size is  $h_i$  and the rate of convergence of the adopted element is  $O(h^l)$  then we can design the new element size to be  $\bar{h}_i$  which is given by the expression

$$\bar{h}_i = \frac{h_i}{\xi_i^{1/l}} \tag{57}$$

The values of  $l$  depends on the smoothness of the solution and on the norm used to evaluate the error. Generally  $l$  is taken to be equal to the polynomial degree of the FE approximation. However, near a singularity it has been shown that  $0.5 \leq l \leq 1$  where the value of  $l$  represents the strength of the singularity (Zienkiewicz and Zhu 1992). Singularities occur in high stress area and the singular point is characterized by high stress and stress gradient values. The relative stress variation is strong in singular areas, and low where the solution is smooth. The location and level of the singularity can be identified by experienced user or based on technique explained by Cugnon and Beckers (1998). Eq. (57) can be used to evaluate the design mesh density for an automatic mesh generator.

---

<sup>2</sup>They introduced a mesh optimality criterion based on the equal distribution of the specific error. In their definition, mesh is optimal if the error per unit area (or volume) is the same over the whole mesh. It is specified that

$$\frac{\|e\|_i}{\Omega_i^{1/2}} = \frac{\|e\|}{\Omega^{1/2}} = \gamma$$

where  $\gamma$  is the required specific error tolerance defined as

$$\gamma \leq \frac{\bar{\eta} \|w^*\|}{\Omega^{1/2}}$$

and  $\Omega_i$  and  $\Omega$  denote the element and total area respectively. The new element refinement parameter is then

$$\xi_i = \frac{\|e\|_i}{\bar{\eta} \|w^*\|} \left( \frac{\Omega}{\Omega_i} \right)^{1/2}$$

### 6.3 Effectivity index

The reliability of the error estimators and various smoothing methods is measured in terms of the effectivity index in the energy norm which is defined as

$$\theta = \frac{\|e\|}{\|\bar{e}\|} = \frac{\text{predicted error}}{\text{actual error}} \quad (58)$$

The error estimator is called asymptotically correct if  $\theta$  converges to continuity when the errors converge to zero (Zienkiewicz and Zhu 1992). In practice, we require that  $\|e\|$  must be close to the actual error  $\|\bar{e}\|$  when the accuracy of the FE solution is in the range of the prescribed values, i.e., when  $\bar{\eta}$  is close to  $\eta$ . For the asymptotically exact error estimators, the bounds of the effectivity index are defined as

$$1 - O(h^\alpha) \leq \theta \leq 1 + O(h^\alpha) \quad (59)$$

For the superconvergent patch recovery method presented above, numerical examples shows that  $\alpha \geq 0.5$  for bi-quadratic elements (Zienkiewicz and Zhu 1992).

## 7. Mesh re-design

Another main ingredient of the AMR procedure is automatic mesh generation and remeshing. Remeshing may involve either refining or coarsening the previous mesh.

The following methods can be used to generate new meshes:

- *Adaptive mesh refinement (AMR)*: In this technique the mesh on which the error was computed is completely discarded and a new mesh of the required density is generated.
- *Mesh enrichment (MER)*: In this method, groups of elements are refined by splitting them and other groups are de-refined by uniting the elements in these groups.
- *Uniform mesh refinement (UMR)*: In this method only uniform meshes are used throughout the domain. The level of refinement is purely based on the global target error.
- *Mesh movement or node relocation (NER)*: In this technique the original topology of the mesh is retained in all analyses. Only the location of the nodal points is changed. UMR method cannot be considered a suitable tool in an adaptive scheme, but it is listed for completeness. A thorough investigation of these methods for one dimensional problems has been carried out by Sieng (1994). The AMR scheme proved to be the most successful for for a linear, second order boundary value problem, as the final mesh possessed the smallest number of degree of freedom for a specified accuracy.

### 7.1 Automatic mesh generation in AMR procedures

As we have seen, AMR procedures involve the design of nearly optimal meshes with varying element sizes to achieve a prescribed accuracy. The importance of AMR procedures in industrial applications has led to increased research on fully automatic mesh generators, which require only the specification of the boundary and mesh size distribution over the domain. The success of AMR procedures depends to a large extent on the efficient coupling between the adaptive FE analysis and

automatic mesh generation.

The AMR procedure requires a convenient means of prescribing the mesh density over the domain, to generate the so-called *optimal* mesh; however, this type of feature is not commonly available in most mesh generators.

Based on a recent study (Sienz 1994, Peraire *et al.* 1987) the advancing front method appears to be one of the best approaches for mesh generation for problems involving adaptive analysis since it incorporates a remeshing facility to allow the possibility of refinement (or derefinement) coupled with directional refinement and allows a significant variation of mesh spacing throughout the region of interest.

In the present work, the remeshing of the whole domain is performed using a mesh generator described in Sienz (1994) which is ideal for AMR procedures.

### 7.2 Evaluation of new mesh densities

When carrying out an initial FE analysis, the background mesh and the mesh parameters must be specified to generate FE meshes. Generally these mesh parameters are defined intuitively by experience. A judicious choice of mesh parameters in the initial background mesh is necessary for fast convergence of the solution during the AMR procedure. For example, the value of the size parameter  $\delta$  could be taken to be approximately  $L/5$  (depending on the element used) where  $L$  is the largest dimension (e.g. side length) in the domain. After the initial FE analysis new values of  $\delta$  are calculated by the use of an error estimator (and prescribed accuracy) at the nodes of the current mesh using the expression

$$\delta_k = \frac{1}{n_{se_i}} \sum_{i=1}^{n_{se}} \bar{h}_i \tag{60}$$

where  $\bar{h}_i$  is the new element size determined from the adaptive analysis using Eq. (57) and  $n_{se}$  is the total number of elements surrounding the node  $k$ .

Once information concerning the new element sizes -- the mesh density -- has been estimated, it is linked to the mesh generator to perform the desired discretisation by transferring the new element sizes to the nodes of the current mesh or to the boundary of the domain to be discretised. In other words, at a given stage of the analysis, the mesh used in the previous analysis becomes the new background mesh. Thus, in this process, the background mesh changes continually during the adaptive analysis.

## 8. Examples

In the previous sections we described the methodology, which may be used to estimate the error energy norm  $\|e\|$  and evaluate the mesh density for the mesh generator. We now present some applications, where these error estimators have been used. In the figures and tables we use the following notation:

- ZZ(NA) --- Zienkiewicz-Zhu error estimator with nodal averaging,
- ZZ(L) --- flux projection error estimator with local stress smoothing,
- ZZ(G) --- flux projection error estimator with global stress smoothing,

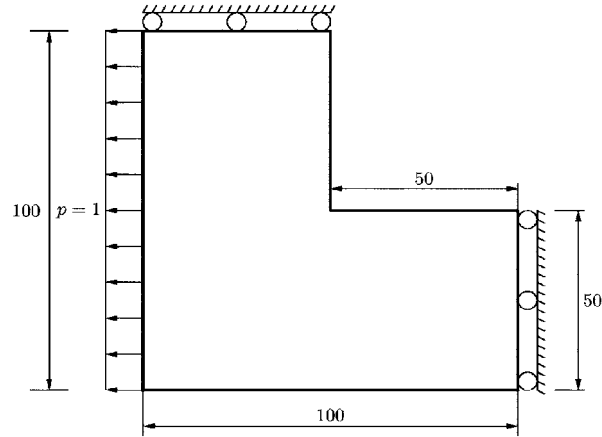


Fig. 3 Geometry of L-shaped plate

- ZZ(LN) --- flux projection error estimator with nodal averaging and Loubignac equilibrium iteration,  
 ZZ(LL) --- flux projection error estimator with local stress smoothing and Loubignac equilibrium iteration,  
 ZZ(S) --- flux projection error estimator with superconvergent patch recovery technique,  
 R(E) --- residual error estimator based on element residual method (the boundary term is neglected),  
 R(S) --- residual error estimator based on sub-domain method,

Three examples are now considered:

- L-shaped plate,
- square plate with symmetrically located central cracks, and
- prism with a square cross-section and a cylindrical hole.

In these examples, self-consistent units are used throughout.

### 8.1 L-shaped plate under edge pressure load

To check that the AMR procedure is working correctly for plane stress problems we consider an L-shaped plate under edge pressure load (Zienkiewicz and Zhu 1992) as shown in Fig. 3. The following properties and dimensions are used: elastic modulus  $E = 100,000.0$ , Poisson's ratio  $\nu = 0.3$ , thickness  $t = 1.0$ , side length  $L = 100.0$  and edge pressure intensity  $p = 1.0$ . The prescribed global percentage error is taken as  $\bar{\eta} = 1\%$ . The values of the strain energy obtained are compared with the exact solution of  $0.311329399$  (Zienkiewicz and Zhu 1992).

We now consider the results:

- The meshes and corresponding error distributions and principal stress plots obtained using ZZ(S) are shown in Fig. 4 for the initial, third, fifth and final iterations.
- The initial mesh of the L-shaped domain shown in Fig. 4 has 20 elements, 103 degrees of freedom, a strain energy  $\|\hat{w}\|_i^2$  equal to 0.305445 and a global percentage error  $\eta = 13.36\%$ .
- After seven iterations, the global percentage error reduces to 0.8831% and the final mesh has 427 elements, 1797 degrees of freedom and strain energy  $\|\hat{w}\|_i^2 = 0.311297$ .

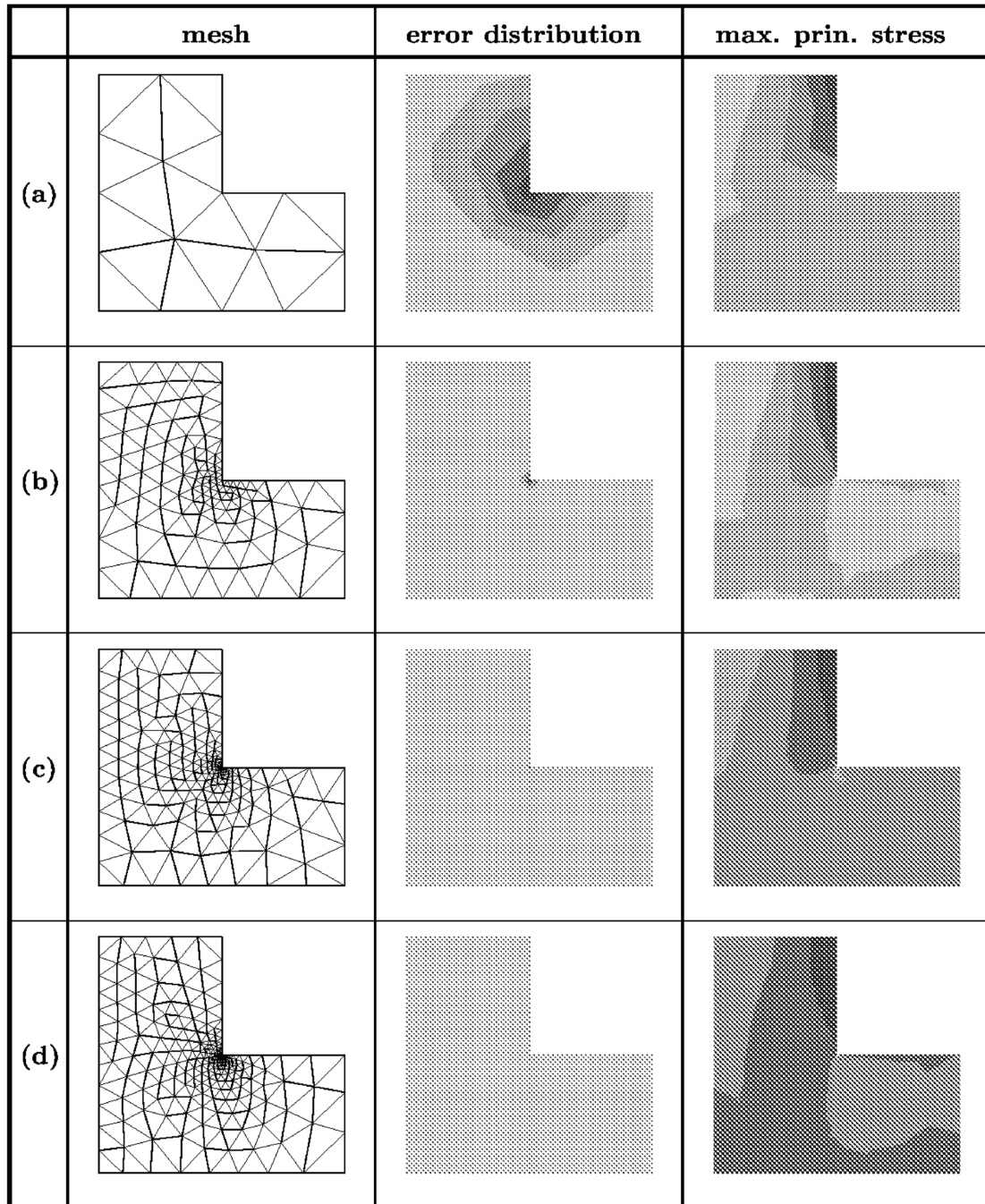


Fig. 4 L-shaped plate --- initial and final meshes and associated error distribution and maximum principal stress obtained using the ZZ(S) method:

(a) first iteration: dof = 106,  $\theta = 0.94$ ,  $\eta = 13.36$ , (b) third iteration: dof = 877,  $\theta = 0.84$ ,  $\eta = 2.65$ ,  
 (c) fifth iteration: dof = 1383,  $\theta = 0.88$ ,  $\eta = 1.25$ , (d) final iteration: dof = 1797,  $\theta = 0.95$ ,  $\eta = 0.88$

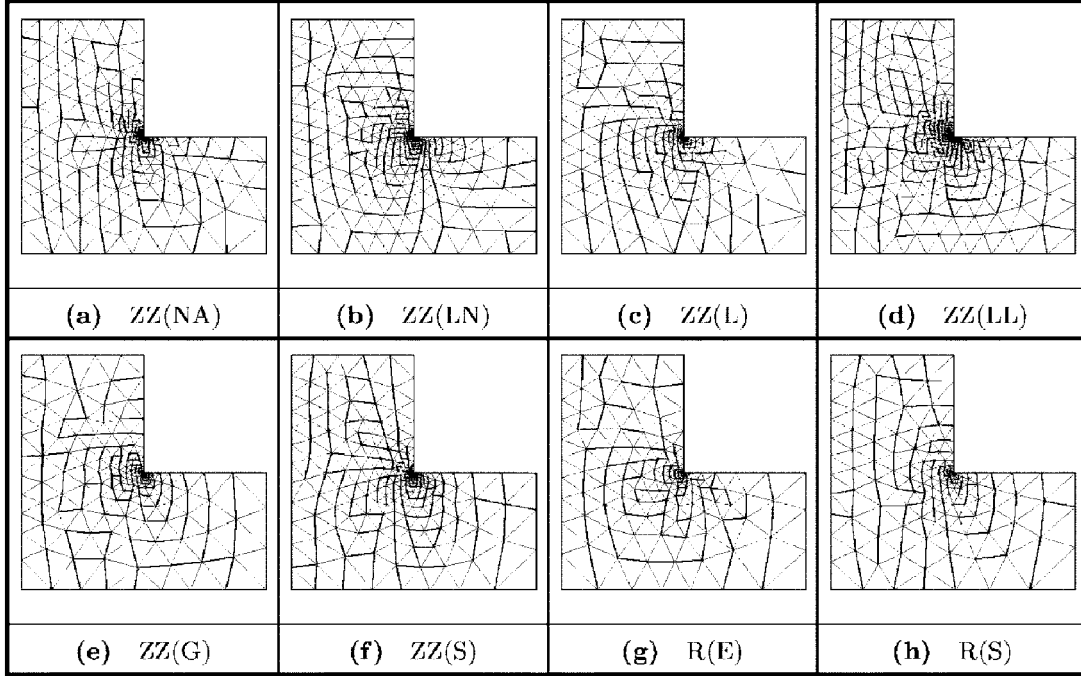


Fig. 5 L-shaped plate --- final meshes obtained using the flux projection error estimator with different stress smoothing methods and residual error estimators:  
 (a) ZZ(NA): dof = 1755,  $\theta = 0.83$ ,  $\eta = 0.87$ ,  
 (b) ZZ(LN): dof = 2389,  $\theta = 1.14$ ,  $\eta = 0.88$ ,  
 (c) ZZ(L): dof = 1469,  $\theta = 0.81$ ,  $\eta = 0.95$ ,  
 (d) ZZ(LL): dof = 2993,  $\theta = 0.97$ ,  $\eta = 0.97$ ,  
 (e) ZZ(G): dof = 1357,  $\theta = 0.76$ ,  $\eta = 0.98$ ,  
 (f) ZZ(S): dof = 1797,  $\theta = 0.95$ ,  $\eta = 0.88$ ,  
 (g) R(E): dof = 1123,  $\theta = 0.86$ ,  $\eta = 0.94$ ,  
 (h) R(S): dof = 1145,  $\theta = 0.91$ ,  $\eta = 0.98$

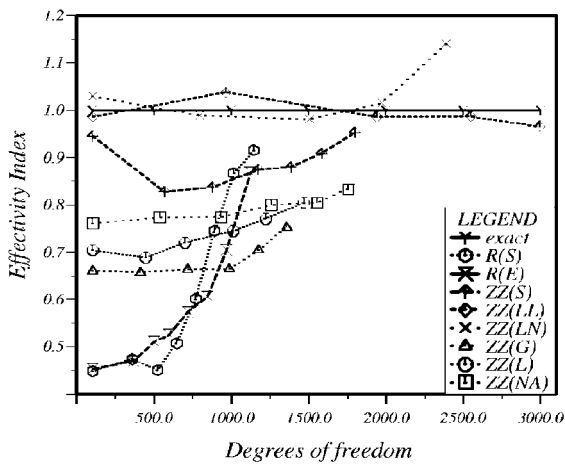


Fig. 6 L-shaped plate: effectivity indices

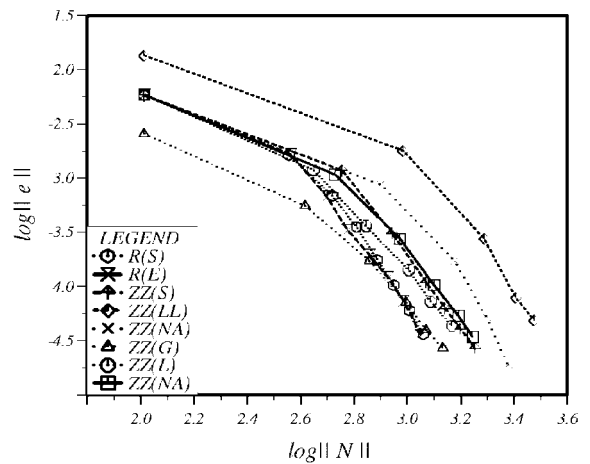


Fig. 7 L-shaped plate: convergence curves for different error estimators

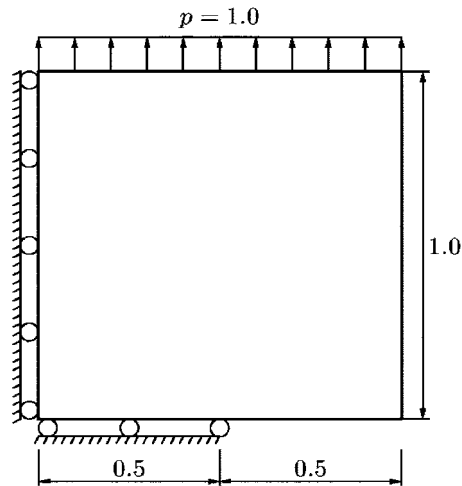


Fig. 8 Geometry of cracked plate problem

- The final meshes obtained using the flux projection and residual based error estimators are shown in Fig. 5. Fig. 6 shows the affectivity indices and Fig. 7 illustrates the corresponding rates of convergence. Note that, the affectivity indices and rate of convergence curves are coincident for the residual methods. Also the rate of convergence curves of the local and global least squares smoothing procedures are identical.
- We achieve the prescribed percentage error of  $\bar{\eta} = 1\%$  for all error estimators and smoothing procedures.

### 8.2 Square plate with symmetrically located central cracks

To demonstrate the efficient use of the AF mesh generator for adaptive FE analysis of plane strain problems and to compare the performance of the different error estimators, we consider a square plate with symmetrically located central cracks under uniform tensile load (Shephard *et al.* 1989) as shown in Fig. 8. The following properties and dimensions are used: elastic modulus  $E = 1.0$ , Poisson's ratio  $\nu = 0.3$ , side length  $L = 2.0$ , length of the crack  $l = 0.5$  and edge pressure intensity  $p = 1.0$ . Prescribed global error percentages of  $\bar{\eta} = 1\%$  and  $\bar{\eta} = 0.5\%$  are assumed for the flux projection and residual error estimators respectively. The exact strain energy for this problem is known to be 1.468762 (Shephard *et al.* 1989).

The results are now presented:

- The initial mesh on the cracked plate domain is shown in Fig. 9 and has 22 elements, 108 degrees of freedom and the strain energy  $||\hat{w}||_i^2$  is equal to 1.400226.
- The initial, third, fifth and final meshes and corresponding error distribution and maximum principal stress are shown in Fig. 9 obtained using the flux projection error estimator with superconvergent patch recovery technique.
- Fig. 10 shows the final meshes obtained with the flux projection error estimator using different smoothing procedures and residual based error estimators.

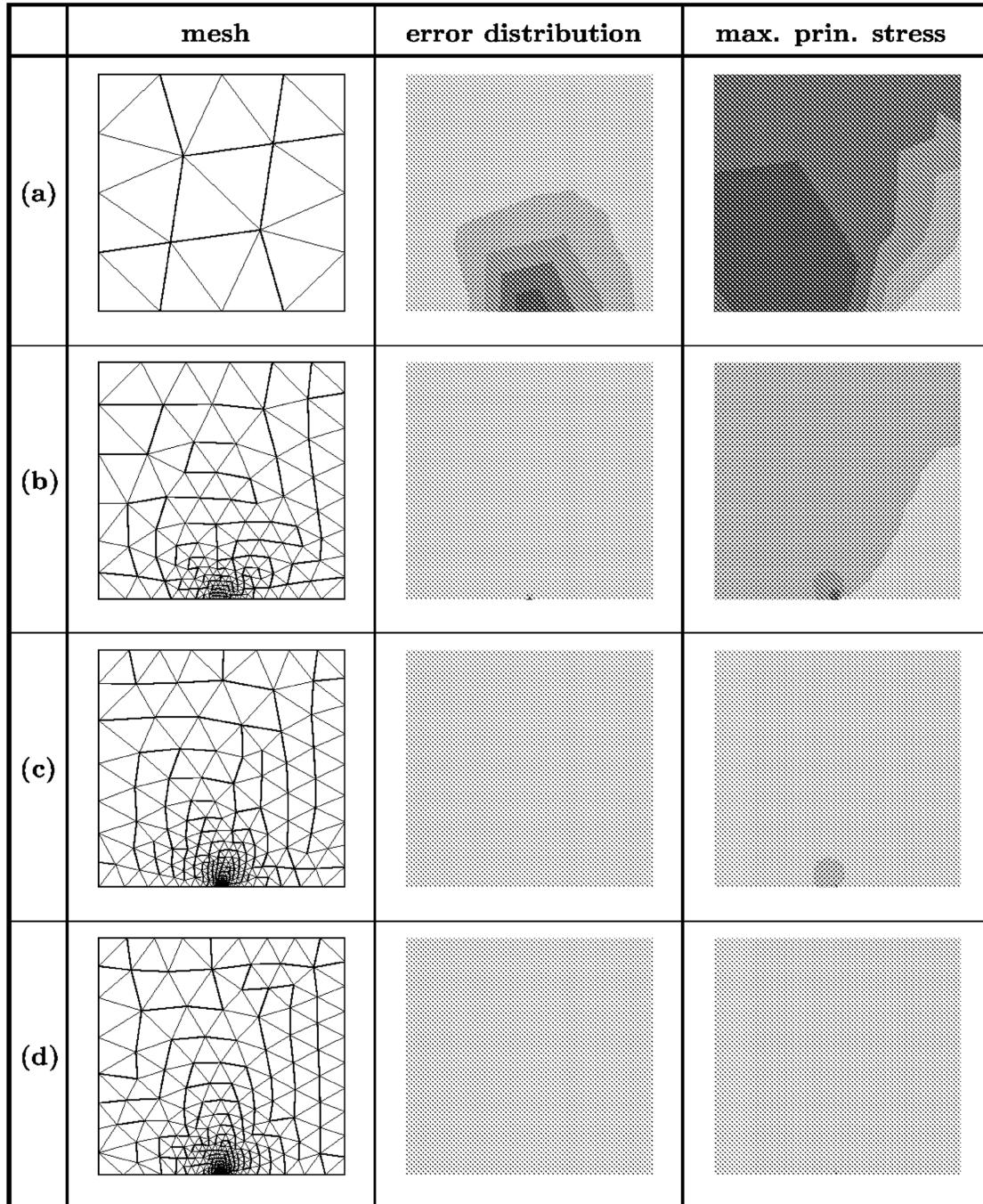


Fig. 9 Cracked plate problem --- Initial and final meshes and associated error distribution and maximum principal stress obtained by the ZZ(S) method:

(a) first iteration: dof = 108,  $\theta = 0.87$ ,  $\eta = 19.96$ , (b) third iteration: dof = 1086,  $\theta = 0.86$ ,  $\eta = 4.18$ ,  
(c) fifth iteration: dof = 1798,  $\theta = 0.90$ ,  $\eta = 1.47$ , (d) final iteration: dof = 2436,  $\theta = 1.12$ ,  $\eta = 0.87$

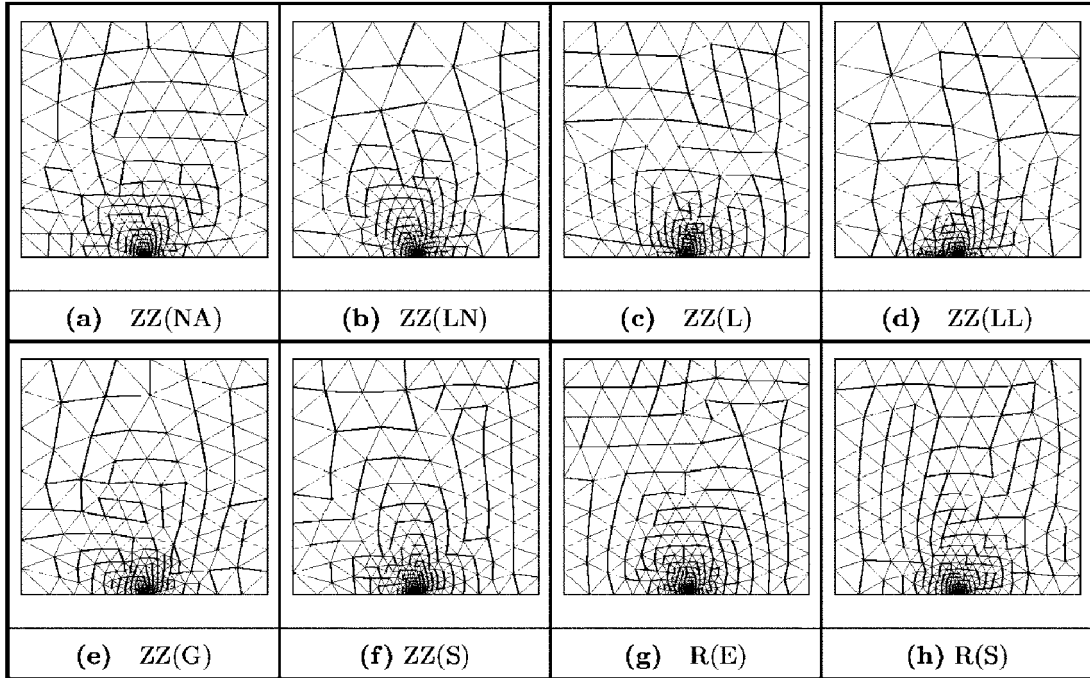


Fig. 10 Cracked plate problem --- final meshes obtained using the flux projection error estimator with different stress smoothing methods and residual error estimators:  
 (a) ZZ(NA): dof = 2052,  $\theta = 0.94$ ,  $\eta = 0.98$ ,  
 (b) ZZ(LN): dof = 1876,  $\theta = 0.97$ ,  $\eta = 1.11$ ,  
 (c) ZZ(L): dof = 2032,  $\theta = 0.81$ ,  $\eta = 0.95$ ,  
 (d) ZZ(LL): dof = 1884,  $\theta = 1.15$ ,  $\eta = 1.23$ ,  
 (e) ZZ(G): dof = 1908,  $\theta = 0.82$ ,  $\eta = 1.00$ ,  
 (f) ZZ(S): dof = 2436,  $\theta = 1.12$ ,  $\eta = 0.87$ ,  
 (g) R(E): dof = 2684,  $\theta = 0.93$ ,  $\eta = 0.45$ ,  
 (h) R(S): dof = 2928,  $\theta = 0.98$ ,  $\eta = 0.49$

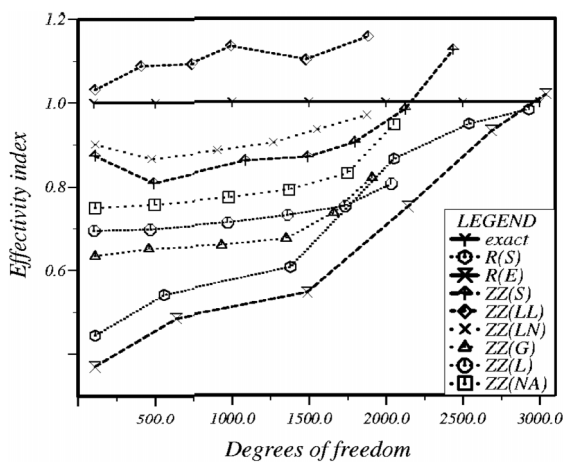


Fig. 11 Cracked plate problem: effectivity indices

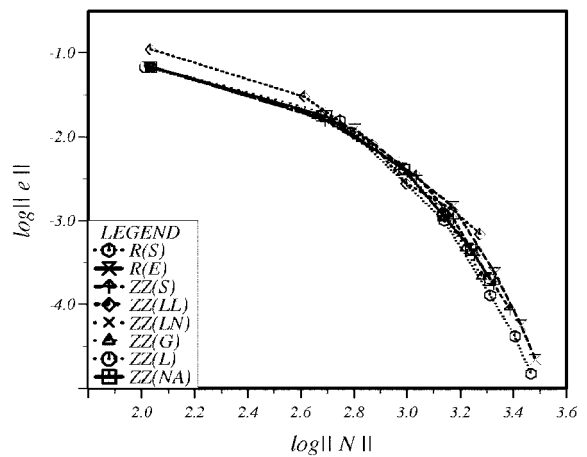


Fig. 12 Cracked plate problem: convergence curves for different error estimators

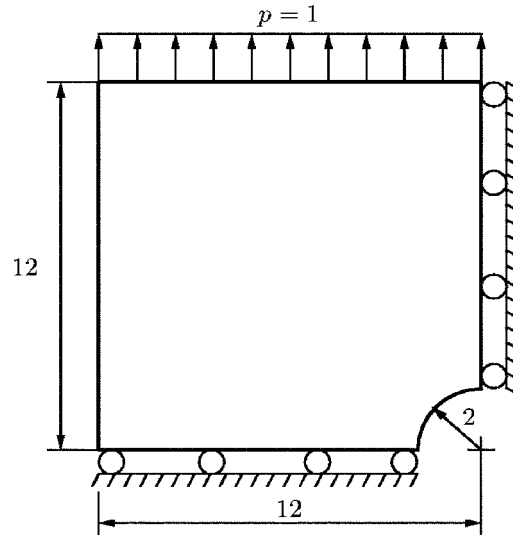


Fig. 13 Prism with a square cross-section and a cylindrical hole

- The comparison of the different methods are given in Figs.11 and 12. Fig.11 shows the effectivity index versus the number of degrees of freedom and Fig.12 illustrates the corresponding rates of convergence obtained.

### 8.3 Prism with a square cross-section and a cylindrical hole

In this third example we deal with a prism with a square cross-section and a cylindrical hole subjected to uniform tensile load. By taking advantage of the double symmetry, which exists in the problem, only a quadrant of the prism is considered. Assuming plane strain condition, Poisson's ratio  $\nu = 0.3$  and elastic modulus  $E = 1.0$ . Other dimensions are indicated in Fig. 13. The pre-specified global percentage error  $\bar{\eta}$  is taken as 0.5%. The values of the strain energy obtained are compared with the exact solution of 1.40333914 (Shephard *et al.* 1989).

The results are now examined:

- The initial mesh contains 30 elements, 179 degrees of freedom giving a strain energy  $\|\hat{w}\| = 1.32732$ .
- Fig. 14 shows the progression of meshes obtained and the associated error distributions and maximum principal stresses using the superconvergent patch recovery technique with pre-specified global percentage  $\bar{\eta} = 0.5\%$ .
- Fig. 15 shows the final meshes obtained using flux projection error estimator with different smoothing procedures and residual type error estimators. The effectivity indices of different error estimators are plotted in Fig. 16. The rates of convergence of the different error estimators are compared in Fig. 17.

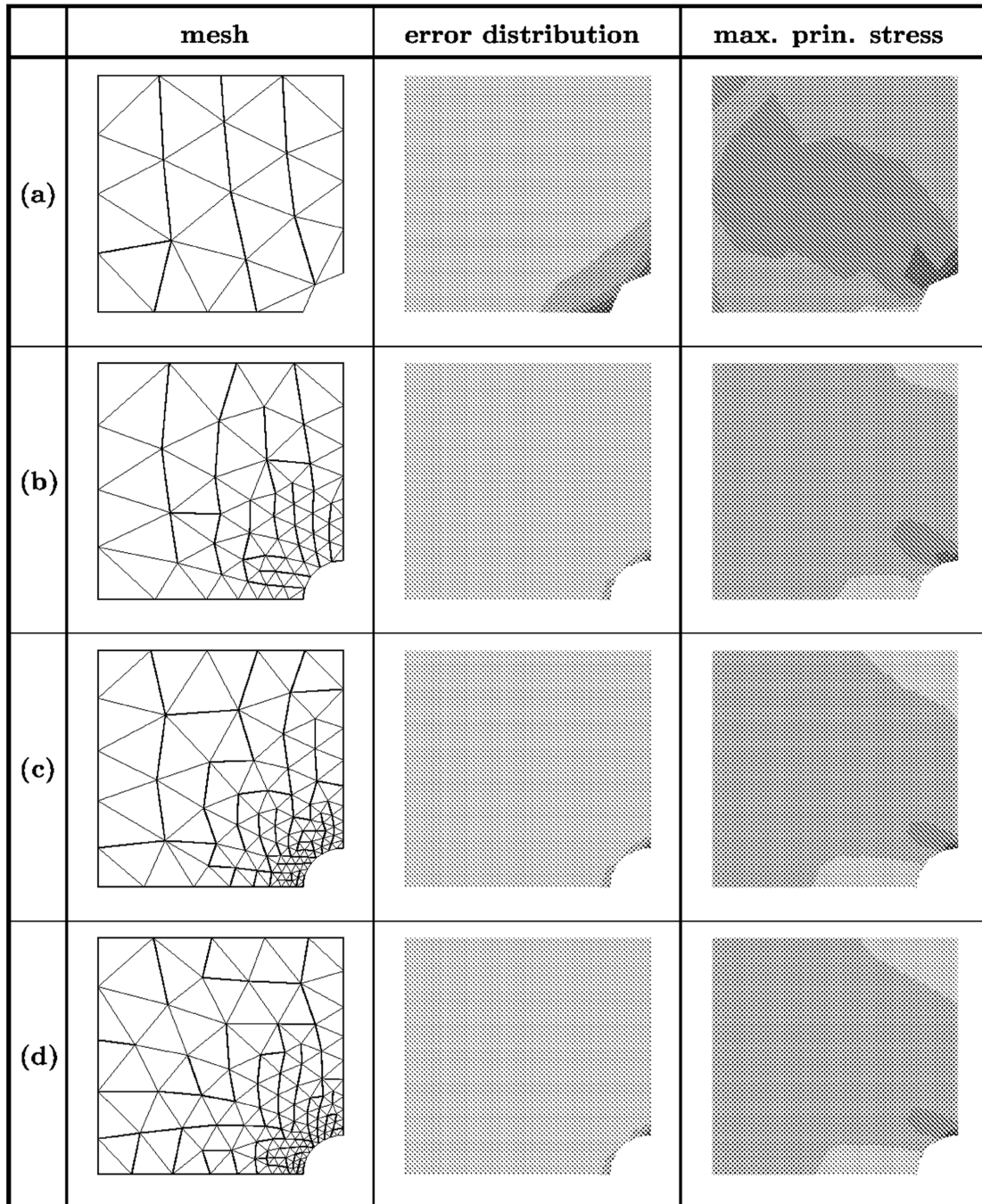


Fig. 14 Prism with a square cross-section and a cylindrical hole --- Initial and final meshes and associated error distribution and maximum principal stress obtained with the ZZ(S) method:

(a) first iteration: dof = 139,  $\theta = 0.60$ ,  $\eta = 6.73$ , (b) second iteration: dof = 433,  $\theta = 0.62$ ,  $\eta = 1.57$ ,  
(c) third iteration: dof = 705,  $\theta = 0.88$ ,  $\eta = 0.53$ , (d) final iteration: dof = 815,  $\theta = 1.04$ ,  $\eta = 0.46$ .

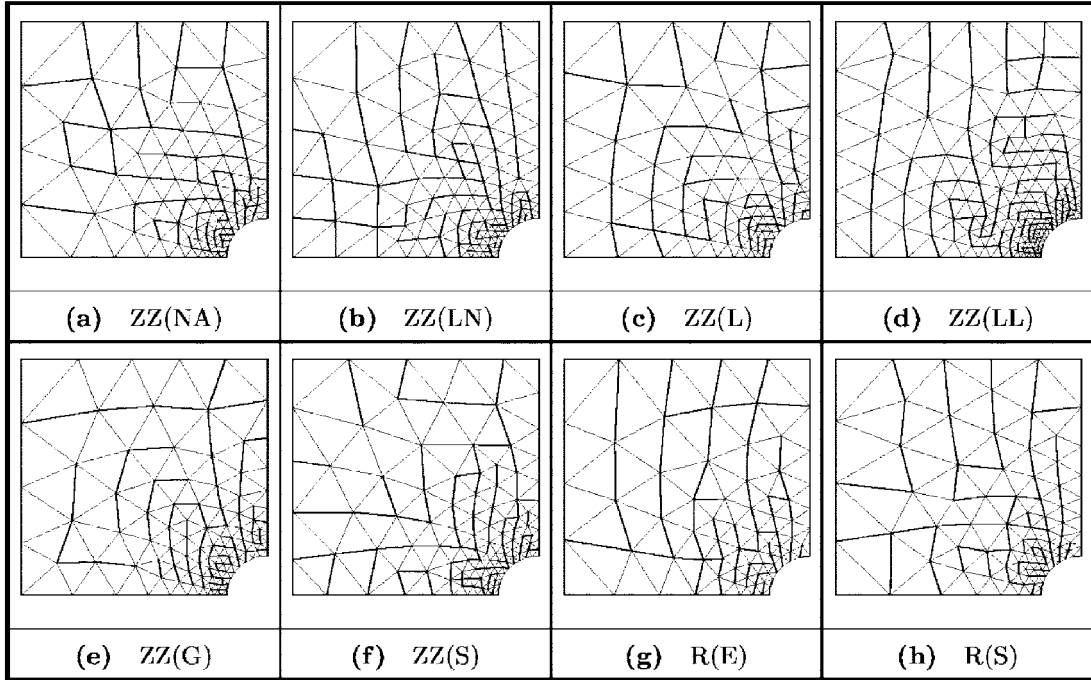


Fig. 15 Prism with a square cross-section and a cylindrical hole --- final meshes obtained using flux projection error estimator with different stress smoothing methods and residual error estimators:  
 (a) ZZ(NA): dof = 779,  $\theta = 0.84$ ,  $\eta = 0.49$ , (b) ZZ(LN): dof = 899,  $\theta = 1.17$ ,  $\eta = 0.45$ ,  
 (c) ZZ(L): dof = 731,  $\theta = 0.71$ ,  $\eta = 0.45$ , (d) ZZ(LL): dof = 1321,  $\theta = 1.15$ ,  $\eta = 0.45$ ,  
 (e) ZZ(G): dof = 779,  $\theta = 0.80$ ,  $\eta = 0.36$ , (f) ZZ(S): dof = 815,  $\theta = 1.04$ ,  $\eta = 0.46$ ,  
 (g) R(E): dof = 547,  $\theta = 0.65$ ,  $\eta = 0.46$ , (h) R(S): dof = 663,  $\theta = 0.93$ ,  $\eta = 0.48$

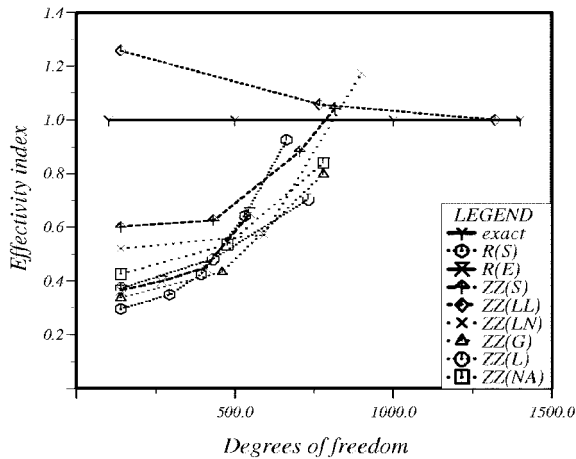


Fig. 16 Prism with a square cross-section and a cylindrical hole: effectivity indices

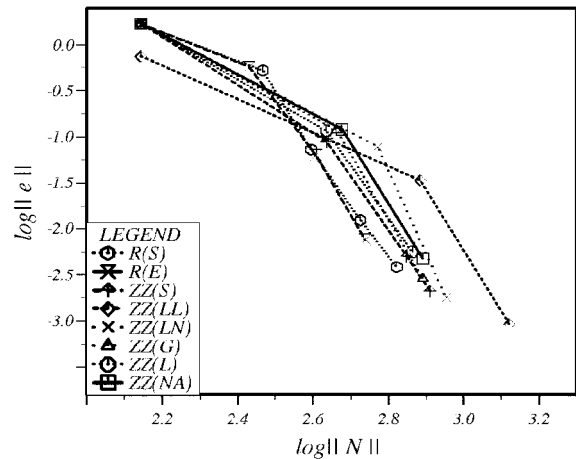


Fig. 17 Prism with a square cross-section and a cylindrical hole: convergence curves for different error estimators

## 9. Conclusions

Based on the above examples the following points are noted.

- The flux projection error estimator with simple nodal averaging, ZZ(NA) has a very high effectivity index value in the first iteration but has a slow convergence to the desired accuracy. It is the easiest method to implement.
- The flux projection error estimator with local smoothing, ZZ(L), gives similar results and a much smaller computational cost when it is compared with global smoothing.
- The use of the flux projection error estimator with global least squares smoothing, ZZ(G), appears to be sufficiently accurate for shape optimisation. Global stress smoothing has slightly better convergence characteristics but a higher computational cost compared to the nodal averaging and local smoothing techniques.
- Simple nodal averaging with Loubignac iteration, ZZ(LN), provides a method for reducing all of the equilibrium errors. The addition of Loubignac iterations improves the values of the effectivity index. However, this method is a relatively expensive procedure. For example to achieve the prescribed accuracy in the L-shaped plate example, the number of degrees of freedom is 2265 as compared to only 1149 degrees of freedom required with the R(S) method. Its use increases the consumed CPU time by a factor of 2 to 3.
- Local smoothing with Loubignac iteration, ZZ(LL), gives the similar results obtained using nodal averaging with Loubignac iteration.
- The superconvergent patch recovery technique, ZZ(S), gives the best convergence and effectivity indices compared with other smoothing procedures. It converges slowly, but it gives better error and mesh distributions.
- The residual method with the higher order bubble shape function, R(S), gives very impressive results giving the best error distribution and the optimal mesh with the smallest number of elements. The rate of convergence of this method is higher than those of other methods. We obtain the desired accuracy using a minimum number of degrees of freedom. However, it is the most complex method from the implementation point of view.
- When we use the residual method, R(E), the results are almost identical to the other residual method, R(S). The effectivity index grows very fast with increasing degrees of freedom and is only slightly greater than 1 at the final iteration. This method is the cheapest error estimation method.

Another aspect of the adaptive process is the selection of  $\bar{\eta}$  (the prescribed accuracy). We only need to obtain a near optimal mesh and hence it is not necessary to give extremely stringent values of  $\bar{\eta}$ . When a very stringent accuracy is prescribed, the number of elements in the final mesh becomes large and also requires more adaptivity iterations to reach that accuracy. An accuracy between 3-8% is reasonable depending on the type of the problem and application.

It has been shown that the number of the elements in the initial mesh greatly influences the rate of convergence and number of the elements in the final optimum mesh. The following strategies can be adopted regarding the selection of the initial mesh:

- Always use a reasonable mesh to start.
- Use judgement and experience to grade the starting mesh.
- Identify points of singularity in the domain.

## References

- Babuska, I. and Rheinboldt, W.C. (1978), "A posteriori error estimates for the finite element method", *Int. J. Num. Meth. Engng.*, **12**, 1597-1615.
- Babuska, I. and Yu, D. (1986), "Asymptotically exact a posteriori error estimator for biquadratic elements", *Technical Note BN-1050*, Institute for Physical Science and Technology, University of Maryland.
- Babuska, I., Strouboulis, T. and Upadhyay, C.S. (1994), "A model study of the quality of a posteriori error estimators for linear elliptic problems, Error estimation in the interior of patchwise uniform grids of triangles", *Comput. Meth. Appl. Mech. Eng.*, **114**, 307-378.
- Babuska, I., Strouboulis, T., Upadhyay, C.S., Gangaraj, S.K. and Copps, K. (1994), "Validation of a posteriori error estimators by numerical approach", *Int. J. Num. Meth. Engng.*, **37**, 1073-1123.
- Baehmann, P.L., Shephard, M.S. and Flaherty, E.J. (1990), "A posteriori error estimation for triangular and tetrahedral quadratic elements using interior residuals", *SCOREC Report*, Scientific Computation Research Center, Rensselaer Polytechnic Institute.
- Barlow, J. (1976), "Optimal stress locations in the finite element method", *Int. J. Num. Meth. Engng.*, **10**, 243-251.
- Cantin, G., Loubignac, G. and Touzot, G. (1978), "An iterative algorithm to build continuous stress and displacement solutions", *Int. J. Num. Meth. Engng.*, **12**, 1493-1506.
- Cho, J.R. and Oden, J.P. (1996), "A priori error estimations of  $hp$  - finite element approximations for hierarchical models of plate and shell like structures", *Comp. Meth. Appl. Mech. Eng.*, **132**, 135-177.
- Cook, R.D., Malkus, S.D. and Plesha, M.E. (1989), *Concepts and Applications of Finite Element Analysis*, 3th ed. John Wiley, New York.
- Cugnon, F. and Beckers, P. (1998), "Error estimation for  $h$ - and  $p$ -method", *8th Mechanical Engineering Chilean Congress* 183-188, 27-30 October.
- Dutta, A. and Ramakrishnan, C.V. (1997), "Error estimation in finite element transient dynamic analysis using modal superposition", *Engineering Computation*, **14**, 135-158.
- Hinton, E. and Campbell, J.S. (1974), "Local and global smoothing of discontinuous finite element functions using a least squares method", *Int. J. Num. Meth. Engng.*, **8**, 461-480.
- Hinton, E., Rock, T. and Zienkiewicz, O.C. (1976), "A note on mass lumping and related processes in the finite element method", *Int. J. Earth. Engng. Struct. Dyn.*, **4**, 245-249.
- Hinton, E., Özakça, M. and Rao, N.V.R. (1991), "An integrated approach to structural shape optimisation of linearly elastic structures Part 2: shape definition and adaptivity", *Computing Systems in Engineering*, **2**, 27-56.
- Hinton, E., Özakça, M. and Rao, N.V.R. (1991), "Adaptive analysis of thin shells using facet elements", *Int. J. Num. Meth. Engng.*, **32**, 1283-1301.
- Kelly, D.W., Gago, J.P. de S.R. and Zienkiewicz, O.C. (1983), "A posteriori error analysis and adaptive processes in the finite element method, Part I: error analysis", *Int. J. Num. Meth. Engng.*, **19**, 1593-1619.
- Mathisen, K.M. and Okstad, K.M. (1999), "Error estimation and adaptivity in explicit nonlinear finite element simulation of quasi-static problems", *Comput. Struct.*, **72**, 627-644.
- Moan, T. (1974), "Optimal polynomials and 'best' numerical integration formulas on a triangle", *ZAMM*, **54**, 501-508.
- Onate, E., Castro, J. and Kreiner, R. (1992), "Error estimation and mesh adaptivity techniques for plate and shell problems", *Proc. of the Third Int. Conf. on Quality Assurance and Standards in Finite Element Analysis*, 1-17.
- Özakça, M. (1993), "Analysis and optimal design of structures with adaptivity", Ph.D thesis, C/Ph/168/93, Dept. of Civil Engineering, University College of Swansea, Swansea, UK.
- Peraire, J., Vahdati, M., Morgan, K. and Zienkiewicz, O.C. (1987), "Adaptive remeshing for compressible flow computations", *J. Comp. Phys.*, **72**, 449-466.
- Robinson, D.J. and Armstrong, C.G. (1992), "An experimental comparison of energy error estimators for 8-noded isoparametric quadrilateral elements", *Proc. of the Third Int. Conf. on Quality Assurance and Standards in Finite Element Analysis*, NAFEM, 202-212.
- Shephard, M.S., Niu, Q.X. and Baehmann, P.L. (1989), "Some results using stress projectors for error indication and estimation", *SCOREC Report*, Scientific Computation Research Center, Rensselaer Polytechnic Institute.

Siensz, J. (1994), "Integrated structural modelling, adaptive analysis and shape optimization", Ph.D. thesis, C/M/259/90, Dept. of Civil Eng. University College of Swansea.  
 Stephen, D.B and Steven, G.P. (1997), "Natural frequency error estimation using a path recovery technique", *J. Sound Vib.*, **200**, 151-165.  
 Strouboulis, T. and Haque, K.A. (1992), "Recent experiences with error estimation and adaptivity, Part 2: error estimation for  $h$  - adaptive approximations on grids of triangles and quadrilaterals", *Comp. Meth. Appl. Mech. Engng.*, **100**, 359-430.  
 Zienkiewicz, O.C. and Zhu, J.Z. (1992), "The superconvergent patch recovery and a posteriori error estimates. Parts 1-2", *Int. J. Num. Meth. Engng.*, **33**, 1331-1382.  
 Zienkiewicz, O.C., Liu, Y.C. and Huang, G.C. (1988), "An error estimate and adaptive refinement method for extrusion and other forming problems", *Int. J. Num. Meth. Engng.*, **25**, 23-42.  
 Zienkiewicz, O.C. and Taylor, R.L. (2000), *The Finite Element Method*, 5th ed., Vols. 1-3, Butterworth Heinemann, London.

### Appendix A. --- Evaluation of residual body forces

The element differential equations of equilibrium for two dimensions can be written as

$$\begin{aligned} \frac{\partial \sigma_x}{\partial x} + \frac{\partial \tau_{xy}}{\partial y} + b_x &= r_x \\ \frac{\partial \sigma_y}{\partial y} + \frac{\partial \tau_{xy}}{\partial x} + b_y &= r_y \end{aligned} \tag{A.1}$$

where  $b_x$  and  $b_y$  are the body forces in the  $x$  and  $y$  direction respectively. For two dimensional problems, the three strain components are

$$\epsilon_x = \frac{\partial u}{\partial x} \quad \epsilon_y = \frac{\partial v}{\partial y} \quad \gamma_{xy} = \frac{\partial u}{\partial y} + \frac{\partial v}{\partial x} \tag{A.2}$$

First, let us consider the residual forces in the element for plane stress problems. In the case of plane stress problem, the constitutive relations for an isotropic material can be written as

$$\begin{aligned} \epsilon_x &= \frac{1}{E}(\sigma_x - \nu\sigma_y) \\ \epsilon_y &= \frac{1}{E}(\sigma_y - \nu\sigma_x) \\ \gamma_{xy} &= \frac{1}{G} = \frac{2(1+\nu)}{E} \tau_{xy} \end{aligned} \tag{A.3}$$

Upon substitution of (A.3) into (A.2) and  $\sigma_x$ ,  $\sigma_y$  and  $\tau_{xy}$  may be evaluated as

$$\begin{aligned} \sigma_x &= \frac{E}{(1-\nu^2)} \left( \frac{\partial u}{\partial x} + \nu \frac{\partial v}{\partial y} \right) \\ \sigma_y &= \frac{E}{(1-\nu^2)} \left( \frac{\partial v}{\partial y} + \nu \frac{\partial u}{\partial x} \right) \\ \tau_{xy} &= \frac{E}{2(1+\nu)} \left( \frac{\partial u}{\partial y} + \frac{\partial v}{\partial x} \right) \end{aligned} \tag{A.4}$$

If we take the derivatives of the stress components with respect to  $x$  and  $y$  and substitute them in (A.1) we obtain the element residual forces for  $x$  and  $y$  directions

$$\begin{aligned} r_x &= \frac{E}{(1-\nu^2)} \left[ \frac{\partial^2 u}{\partial x^2} + \frac{(1-\nu)}{2} \frac{\partial^2 u}{\partial y^2} + \frac{(1+\nu)}{2} \frac{\partial^2 v}{\partial x \partial y} \right] \\ r_y &= \frac{E}{(1-\nu^2)} \left[ \frac{\partial^2 v}{\partial y^2} + \frac{(1-\nu)}{2} \frac{\partial^2 v}{\partial x^2} + \frac{(1+\nu)}{2} \frac{\partial^2 u}{\partial x \partial y} \right] \end{aligned} \quad (\text{A.5})$$

The element residual body force  $r$  can be expressed as

$$r = \sqrt{r_x^2 + r_y^2} \quad (\text{A.6})$$

The residual forces for plane strain problems are

$$\begin{aligned} r_x &= \frac{E}{(1+\nu)} \left[ \left( \frac{1-\nu}{1-2\nu} \right) \frac{\partial^2 u}{\partial x^2} + \frac{\nu}{(1-2\nu)} \frac{\partial^2 v}{\partial x \partial y} + \frac{1}{2} \left( \frac{\partial^2 u}{\partial y^2} + \frac{\partial^2 v}{\partial x \partial y} \right) \right] \\ r_y &= \frac{E}{(1+\nu)} \left[ \left( \frac{1-\nu}{1-2\nu} \right) \frac{\partial^2 v}{\partial y^2} + \frac{\nu}{(1-2\nu)} \frac{\partial^2 u}{\partial x \partial y} + \frac{1}{2} \left( \frac{\partial^2 v}{\partial x^2} + \frac{\partial^2 u}{\partial x \partial y} \right) \right] \end{aligned} \quad (\text{A.7})$$

and for axisymmetric problems

$$\begin{aligned} r_r &= \frac{E}{r(1-\nu^2)} \left[ r \frac{\partial^2 u}{\partial r^2} + \frac{\partial u}{\partial r} + \frac{(1-\nu)}{r} \frac{\partial^2 u}{\partial \theta^2} - \frac{u}{r} + \frac{(1+\nu)}{2} \frac{\partial^2 v}{\partial r \partial \theta} - \frac{(3-\nu)}{2r} \frac{\partial v}{\partial \theta} \right] \\ r_\theta &= \frac{E}{r(1+\nu)} \left[ \frac{3-\nu}{2(1-\nu)} \frac{\partial^2 u}{\partial r \partial \theta} + \frac{3-\nu}{2r(1-\nu)} \frac{\partial u}{\partial \theta} + \frac{1}{r(1-\nu)} \frac{\partial^2 v}{\partial \theta^2} + \frac{r}{2} \frac{\partial^2 v}{\partial r^2} + \frac{1}{2} \left( \frac{\partial v}{\partial r} \frac{\partial v}{\partial r} \right) \right] \end{aligned} \quad (\text{A.8})$$